Agricultural Water Management 267 (2022) 107628

Contents lists available at ScienceDirect

Agricultural Water Management

journal homepage: www.elsevier.com/locate/agwat

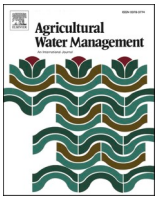

Assessment of peach trees water status and leaf gas exchange using on-the-ground versus airborne-based thermal imagery

J.M. Ramírez-Cuesta [a,*], M.F. Ortuño [b], V. Gonzalez-Dugo [c], P.J. Zarco-Tejada [c,d], M. Parra [b], J.S. Rubio-Asensio [b], D.S. Intrigliolo [a]

[a] Department of Ecology, Desertification Research Centre (CIDE-CSIC-UV-GV), Moncada, Valencia 46113, Spain
[b] Centro de Edafología y Biología Aplicada del Segura (CEBAS), Consejo Superior de Investigaciones Científicas (CSIC), Espinardo, 30100 Murcia, Spain
[c] Instituto de Agricultura Sostenible (IAS), Consejo Superior de Investigaciones Científicas (CSIC), Alameda del Obispo s/n, 14004 Cordoba, Spain
[d] School of Agriculture and Food (SAF-FVAS) and Faculty of Engineering and Information Technology (FEIT), University of Melbourne, Melbourne, Victoria, Australia

ARTICLE INFO

Handling Editor - J.E. Fernández

Keywords:
Physiological parameters
Remote sensing
Thermography
Canopy temperature

ABSTRACT

The thermal region of the electromagnetic spectrum might provide valuable information for assessing plant water status. Nevertheless, the plant's physiology and the scale of measurement, (e.g. sensor viewing geometry and the canopy aggregation) are critical for quantifiying and monitoring water stress. This study compares the Crop Water Stress Index (CWSI) of a peach orchard obtained using on-the-ground, and airborne-based canopy temperature (T_c). The temporal evolution of CWSI under mild water stress conditions was assessed for three different irrigation strategies (over-irrigation, OI; farmer irrigation, FI; and non-irrigation, NI). Two aerial campaigns per irrigation season (2017–2018) were performed with an airborne thermal sensor: a first flight under well-watered conditions, and a second flight once mild water stress was developed. At the time of the flights, T_c and net photosynthesis (P_n), stomatal conductance (g_s) and stem water potential (Ψ_s) were measured on the ground with a hand-held thermal camera, a portable gas exchange system and a pressure chamber, respectively. The canopy temperature obtained from the hand-held thermal camera, averaging the sunlit and shaded parts of the canopy, agreed with that derived from the airborne measurements (Y=1.00X; RMSE= 1.97 K). The CWSI values calculated from both approaches detected peach water status under different irrigation strategies. In general, Ψ_s was better predicted from the aircraft (R^2 up to 0.72 for CWSI obtained from the aircraft versus R^2 =0.51 for T_c ground measurements), whereas the use of ground measurements was preferred for estimating g_s and P_n (R^2 up to 0.73 and 0.74 for T_c ground measurements versus R^2 =45 and 0.56 for T_c and CWSI derived from the aircraft). Regardless the approach used for deriving T_c, and due to the consideration of different meteorological conditions (i.e different dates), CWSI provided a better relationship with Ψ_s than T_c, whereas the latter was more closely related with g_s and P_n.

1. Introduction

Understanding the main effects of water stress on plant water status is required in order to define adequate scheduling irrigation for reducing the negative impacts of drought on tree growth and production (Steduto et al., 2012). Thus, in recent years, there has been a great interest in searching for plant-based water status indicators alternative to the stem water potential, which is considered the standard for plant-based irrigation management and for water stress assessment (García-Tejera et al., 2021; Shackel et al., 2021). In this sense, canopy temperature has been generally accepted as a reliable and non-invasive indicator of crop water stress by capturing the limitation of the dissipation of the latent heat flux by plant transpiration (Tanner, 1963; Gates, 1964). However, the possibility of determining plant water status from canopy determinations depends on the plant's physiological responses to soil water deficit (i.e. isohydric versus anisohydric behaviors), leaf anatomy (large versus lanceolate leaves) and the environmental conditions, particularly the wind speed (Jones, 2004a, 2004b).

Leaf temperature measurement has been usually performed on the ground with infrared radiometers, hand-held thermal guns, and camera thermography. However, one of the main problems of the use of on-ground indicators is that, due to its punctual nature, a large number of

* Corresponding author.
E-mail addresses: ramirezcuesta.jm@gmail.com, jm.ramirez.cuesta@csic.es (J.M. Ramírez-Cuesta).

https://doi.org/10.1016/j.agwat.2022.107628
Received 30 October 2021; Received in revised form 11 March 2022; Accepted 24 March 2022
Available online 30 March 2022

measurements covering the entire study area are needed to properly characterize the spatial variability of the crop water status among trees within an orchard (due to variability in both soil volume explored and tree foliar surface) and within a single tree canopy (Cohen et al., 2005; Ngao et al., 2017). This variability depends on many factors, including physical-chemical properties of soils (texture, depth, nutrients, organic matter, etc.), plant morphology (canopy size and architecture), field topography, existence of microclimates or the presence of pathogens, among others (Starr, 2005).

The limitations indicated above can be overcome with the development of recent technological advances in remote sensing in the thermal domain. New compact thermal cameras allow capturing spatial surface temperature data, thus facilitating the mapping of canopy temperature variability over the entire plot non-invasively (Cohen et al., 2005; Ortega-Farías et al., 2016). However, contrary to ground-measured T_c measurements collected below the clouds, the use of remote sensing for determining T_c, specifically from satellites, is limited only to clear-sky conditions, additionally requiring the absence of wind in the case of airborne thermal imaging (Agam et al., 2013).

The accuracy of surface temperature retrievals from remote sensing is quite dependent on sensor calibration, atmospheric attenuation and sourcing, surface emissivity, view angle, and shadowing (Norman et al., 1995). Moreover, its accuracy also depends on the platform used for acquiring the image, ranging from 1 to 2 K, when using satellite data (Wan, 2014; Sobrino et al., 2020); and reaching accuracies lower than 1 K when manned aircraft or drones are used (Sepulcre-Cantó et al., 2006; Berni et al., 2009; Ramírez-Cuesta et al., 2017).

The use of T_c as a water status indicator requires normalization to account for the varying environmental conditions (Idso et al., 1981). To deal with it, T_c can be used in combination to air temperature (T_a) as an indicator of water status. This has been explored since the pioneering work by Idso et al. (1981), which described the Crop Water Stress Index (CWSI). This index was specifically developed for fully covering crops, but the improvements in the spatial resolution of thermal sensors during the last decades have allowed its application to row crops. The computation of CWSI requires the use of two anchor thresholds to normalize for the effects of atmospheric conditions on transpiration and canopy temperature (King et al., 2021). These thresholds correspond to fully transpiring (lower limit; LL), and non-transpiring (upper limit; UL) conditions, respectively.

Initially, LL and UL were determined using natural references, i.e. crop regions maintained under fully transpiring and non-transpiring conditions (Clawson et al., 1989; Jones, 1999b; Jones et al., 2002). However, determining the natural references still remains a challenge in practical conditions due to the lack of uniformity and reproducibility, and to the difficulty in achieving and maintaining such anchor canopy conditions (Cohen et al., 2005; Möller et al., 2007; King et al., 2021).

Alternative methods of estimating LL and UL have been proposed in the literature. Thus, an example is the use of artificial reference surfaces (Alchanatis et al., 2010; O'Shaughnessy et al., 2011; Pou et al., 2014). In such approach, UL is set to Ta + 5 ºC (value found as the maximum leaf temperature under several conditions according to Cohen et al., 2005, Irmak et al., 2000 and Möller et al., 2007); whereas the lower limit is determined based on reference measurements of a wet artificial reference surface captured by the thermal image. However, the high sensitivity of CWSI to the value assigned to UL and the need for capturing a wet reference in every analysed image have been highlighted as the main limitations of this empirical approach (Ben-Gal et al., 2009).

Even if these drawbacks limit the usefulness of empirical CWSI for routine measurements (Agam et al., 2013), the use of natural and artificial references has allowed researchers to successfully capture water status in soybean (O'Shaughnessy et al., 2011), cotton (Cohen et al., 2005; O'Shaughnessy et al., 2011), grapevines (Möller et al., 2007) and olives (Ben-Gal et al., 2009), among other crops.

Another alternative to the empirical determination of CWSI thresholds is their analytical calculation based on the canopy energy balance (Jackson et al., 1981, 1988; Jones, 1999a). Nonetheless, contrary to empirical approaches, theoretical formulation requires meteorological data (e.g. incoming solar radiation, air temperature, relative humidity, and wind speed) for the estimation of net radiation and aerodynamic resistance, which can result in high uncertainties in the CWSI calculation (Ben-Gal et al., 2009). Moreover, several authors have indicated that a theoretical LL and UL formulation is limited by the complexity of the canopy architecture (particularly in woody crops) and the influence of environmental conditions in the soil-plant-atmosphere continuum (Idso et al., 1981; Jones, 1999a, 2004; King et al., 2021).

The determination of these thresholds is also subjected to the uncertainty caused by the tree crown subcomponent selection to carry out the measurements. For instance, when obtaining thermal imagery from remote sensing (e.g. UAVs or aircrafts), the thermal sensor measures the temperature of the upper part of the tree, which has warmer and more sun-exposed leaves than the tree as a whole (Ngao et al., 2017; González-Dugo et al., 2012). On the contrary, when performing the measurements on the ground, T_c varies depending on the side of the tree where the measurements are taken. Thus, the validity of UL and LL obtained from remote sensing measurement needs to be carefully checked when combined to ground T_c measurements.

One of the main limitations of ground and airborne thermography refers to the instantaneous nature of thermal sensors, which provide measurements at a certain moment. The quick temporal variability of T_c could make that the instantaneous T_c acquired by the sensor differs considerably from one moment to another, which would severely affect the intercomparison between measurements taken at different times (i.e. in different thermal images). Specifically, Peters and Evett (2004); and Reddy et al. (2015) found T_c variations of up to 2–4 ºC, respectively, in a 30-min period.

Several studies have shown accurate relationships of crop water stress indicators with physiological parameters in heterogeneous crops, including vineyards (Möller et al., 2007; Baluja et al., 2012; King and Shellie, 2016; Sepúlveda-Reyes et al., 2016; Santesteban et al., 2017; Poblete et al., 2018), citrus (Gonzalez-Dugo et al., 2014), almond (Camino et al., 2018), pistachio (Gonzalez-Dugo et al., 2015), olive (Ben-Gal et al., 2009) and peach (Bellvert et al., 2016), among others.

To the best of our knowledge, no studies have been conducted on the direct evaluation of on-the-ground versus airborne-level CWSI calculations for assessing crop water stress in an orchard (Jamshidi et al., 2021; Ben-Gal et al., 2009). This is critical for identifying the main strengths and limitations of each approach and for helping to select the most appropriate method depending on the crop-site specificities. The relationships between canopy temperature taken from different sources and several physiological indicators of plant water status need to be explored to assess the implications of different T_c quantifications.

The main objective of this research is to check the suitability of two methodologies, on-ground and remote-based thermal imaging, for identifying mild water stresses in a peach orchard. In particular, this objective was addressed by (i) assessing the correlation between CWSI and midday stem water potential and leaf gas exchange parameters; and (ii) evaluating whether the LL and UL appropriate for one of the methodologies are also appropriate for the other or whether they need to be modified.

2. Materials and methods

2.1. Study site and irrigation strategies

The experiment was performed in 2017–2018 in a peach orchard (*Prunus persica* var. Amandine) of 3.4 ha located in Murcia, southeastern Spain (38°06′N, 1°12′W). Trees were planted in 2013 with a NW-SE row orientation and a planting framework of 5 × 3.5 m. Mean (± standard deviation) canopy diameter and tree height were 3.3 m (± 0.4 m) and 2.4 m (± 0.1 m), respectively. Trees were drip irrigated with one irrigation line resulting in a density of 6 drippers with a flow rate of

3.2 L h^{-1} per tree. The electrical conductivity of the irrigation water was 2.2 dS m^{-1} and the soil in the area was clay loam. The climate in the study area is semi-arid Mediterranean, with an average air temperature and relative humidity of 18.0 °C (minimum of 2.4 ºC and maximum of 30.9 ºC) and 55.8% (minimum of 22.7% and maximum of 86.8%), respectively; and a cumulative yearly precipitation and reference evapotranspiration of 306 and 1411 mm yr^{-1}, respectively, for the period 2017–2018 (Weather station code MO22; http://siam.imida.es).

The suitability of on-ground and remote thermal sensing-based methods for identifying mild water stress in the study area was tested. The effect of three irrigation strategies applied prior to the development of stress was evaluated: (i) Farmer irrigation (FI), where the trees were irrigated for replacing 100% ET_c until harvest, adopting a late, mild deficit irrigation strategy in order to save water and cope with the chronic water scarcity in the area; (ii) over irrigating 7 days before the initial flight of each season to ensure non-water stress initial conditions (OI), by duplicating the number of drippers; and (iii) non-irrigation (NI), where the trees were not irrigated on the 7 days prior to the initial flight of each season (Fig. S1).

Each irrigation treatment was applied to a tree line, keeping one border line between the different irrigation treatments. For each irrigation strategy, three trees were selected as sample trees (Fig. 1).

2.2. Airborne campaigns

Two airborne remote sensing campaigns at the post-harvest period were performed per year (2017 and 2018; Table 1) employing a Cessna C172S aircraft operated by the Laboratory for Research Methods in Quantitative Remote Sensing (QuantaLab, IAS-CSIC, Spain). Flights were carried out at solar midday time at 200 m above ground level (AGL). The first flight was carried out under overall well-watered conditions, except for the NI treatment, which was not irrigated in the previous 7 days (t_0; Fig. S1); whereas the second flight was performed once mild water stress developed (t_1; Fig. S1). Soil water deficit was imposed by withholding irrigation for 3–4 days before the second thermal image acquisition for FI and OI; and no irrigation conditions were maintained for NI (Table 1; Fig. S1).

Table 1
Dates (and daily reference evapotranspiration, ET_0, mm d^{-1}) of the flight campaigns. ET_0 was retrieved from a weather station located 1.5 km far from the study site (Code MO22, http://siam.imida.es).

Year	Condition	Date[a]	ET_0 (mm d^{-1})	Ψ_s[b] (MPa)	T_a (K)	VPD (kPa)
2017	Well-watered	18 Jul	6.5	[− 0.98, − 2.33]	305.99	2.61
	Mild water stress	24 Jul (20 Jul)	6.5	[− 1.88, - 2.20]	306.68	2.55
2018	Well-watered	02 Jul	8.6	[− 1.02, − 1.95]	306.29	2.94
	Mild water stress	06 Jul (03 Jul)	6.6	[− 1.62, − 1.92]	303.84	2.36

[a] The date of irrigation withholding is indicated in brackets.
[b] Ψ_s interval refer to: [over irrigated (OI) treatment, non-irrigation (NI) treatment]

Canopy temperature was acquired from a thermal sensor on board the aircraft. The thermal sensor was a FLIR SC655 thermal camera (FLIR Systems, Wilsonville, OR, USA), which acquires images in the 7.5–13 μm range with a resolution of 640 × 480 pixels, and an optics focal length of 13.1 mm that yields an angular FOV of 45° and a spatial resolution of 25 cm (Fig. 1). This sensor has a thermal sensitivity and an absolute accuracy of < 0.05 K (at 303.15 K) and ± 2 K, respectively. Thermal images were radiometrically, atmospherically and geometrically corrected. For further information about sensor setting and calibration, see Zarco-Tejada et al. (2012) and Ramírez-Cuesta et al. (2019).

Thermal images were mosaicked using Pix4D software (Pix4D, Lausanne, Switzerland). Additionally, in order to extract the canopy temperature from the crowns, segmentation of pure vegetation and bare soil surfaces was performed by delineating isotherms at 0.1 K intervals with ArcGIS (v. 10.5; Esri, Redlands, CA, USA). Thus, a temperature threshold was visually selected in the transition area between both

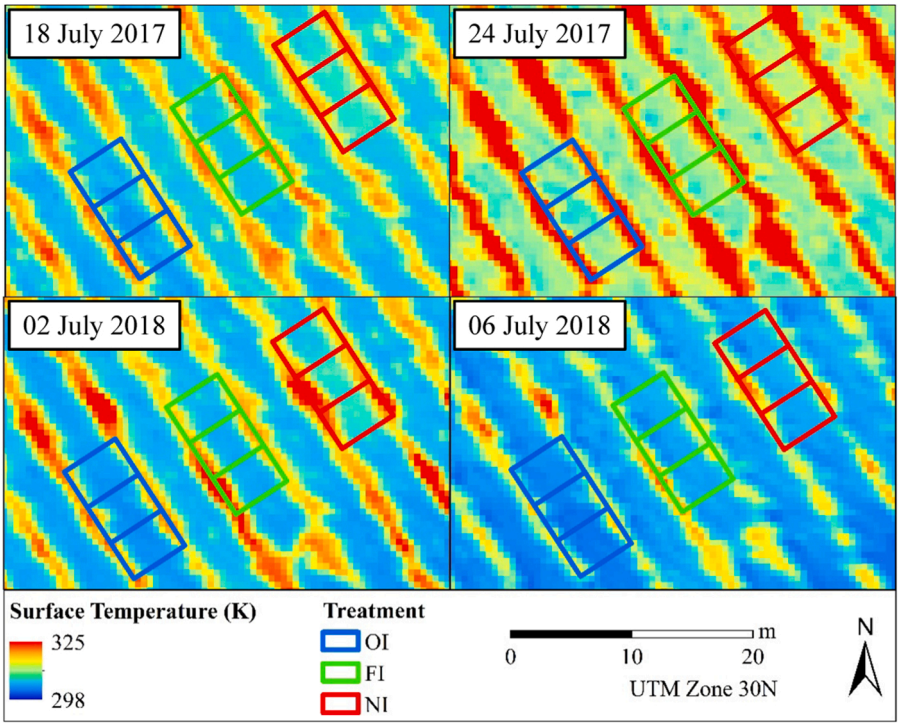

Fig. 1. Surface temperature (K) images obtained from airborne under overall well-watered (18 July 2017 and 02 July 2018) and mild water stress conditions (24 July 2017 and 06 July 2018). OI, FI and NI refer to over irrigation, farmer irrigation and non-irrigation treatments, respectively.

surface types, (i.e. where the isotherms were closer to each other). The identification of the 9 individual trees (3 per treatment) was performed using a fishnet methodology that created a mesh that was applied in all flights in order to obtain the same identifier for each tree.

2.2.1. Crop water stress index calculation

The Crop Water Stress Index calculated from the airborne thermal imagery ($CWSI_a$) was calculated as follows (Idso et al., 1981):

$$CWSI_a = \frac{(T_{c,a} - T_a) - (T_c - T_a)_l}{(T_c - T_a)_u - (T_c - T_a)_l} \quad (1)$$

where $T_{c,a}$ is the canopy temperature calculated as the average of the pure vegetation pixels within a tree; T_a is the air temperature recorded at the time of the measurements obtained from the nearest weather station; $(T_c\text{-}T_a)_l$ is the lower baseline representing a canopy transpiring at the potential rate; and $(T_c\text{-}T_a)_u$ is the upper baseline referring to a canopy where transpiration is completely stopped. Since CWSI considers canopy to air temperature differences, temperatures can be expressed in K or ºC, but must be consistent for all terms. This index ranges from values close to 0 (when the crop is fully watered) to 1 (when the crop is under severe water stress conditions). In this study, the lower baseline utilised was the one proposed by Berni et al. (2012) (i.e. $(T_c\text{-}T_a)_l = -1.57 * VPD + 3.25$); whereas the upper baseline was set as $T_a + 5$ K, (or ºC, depending on T_a units) as suggested by Irmak et al. (2000).

2.3. Ground measurements

2.3.1. Canopy temperature and CWSI

A hand-held thermal camera (ThermaCam FLIR-e50 System, Inc., Danderyd, Sweden) was used to collect thermal images of the sunlit part of the tree canopy in three trees per irrigation treatment at the time of the airborne campaigns (Figs. 2 and 3). This camera operates in the 7.5–13 μm electromagnetic region with a 240 × 180-pixel line scan imager, providing a thermal sensitivity and an absolute accuracy of < 0.05 K (at 303.15 K) and ± 2 K, respectively.

Two thermal images per tree and irrigation treatment (n = 6 per treatment) were taken from the sunlit side of the canopy at a constant distance of 1.5 m from the plant canopy and at a constant height of 1.6 m (see T_c boxes in Fig. 4). Each thermal image approximately covered an area of 0.70 × 0.70 m.

The background temperature was established to discard the effect of the radiation originating from other objects that reflects off the target being measured (Costa et al., 2013). It was determined as the temperature of a crumpled aluminium sheet placed in a similar position to the area of interest and setting the emissivity at 1.0 (Jones et al., 2002). Emissivity for leaf measurements was assumed as 0.96 (Jones, 2004a, 2004b; Grant et al., 2006).

The ThermaCam Explorer software (FLIR Quick Report, FLIR Systems, Danderyd, Sweden) was used for processing thermal images. For each thermal image, five sunlit areas (30 per treatment) were manualy identified (Fig. 4), which were averaged to obtain a global T_c value. These T_c images obtained from the sunny side were used to establish the correlation with the physiological parameters measured in the same trees (see "2.3.2. Physiological determinations"). In addition to the T_c images acquired on the sunny side, another two T_c images per tree were taken on the shaded side (similarly to T_c boxes in Fig. 4) in order to evaluate the T_c pattern within the plant.

For the comparison between the T_c obtained from the hand-held thermal camera ($T_{c,g}$) (both in the sunlit and shaded sides of the trees) and the $T_{c,a}$, the percent BIAS (PBIAS) statistical indicator was used. This indicator provides insights into the aircraft-derived data to be larger or smaller than their corresponding on-ground data, calculated as:

$$PBIAS \quad (\%) = 100 * \frac{\sum_{i=1}^{n}(T_{c,g} - T_{c,\ \ a})}{\sum_{i=1}^{n}(T_{c,g})} \quad (2)$$

where *n* is the number of sampled trees. Positive values of PBIAS imply that the determinations at the airborne level underestimates the on-ground values, and vice versa (Fandiño et al., 2015).

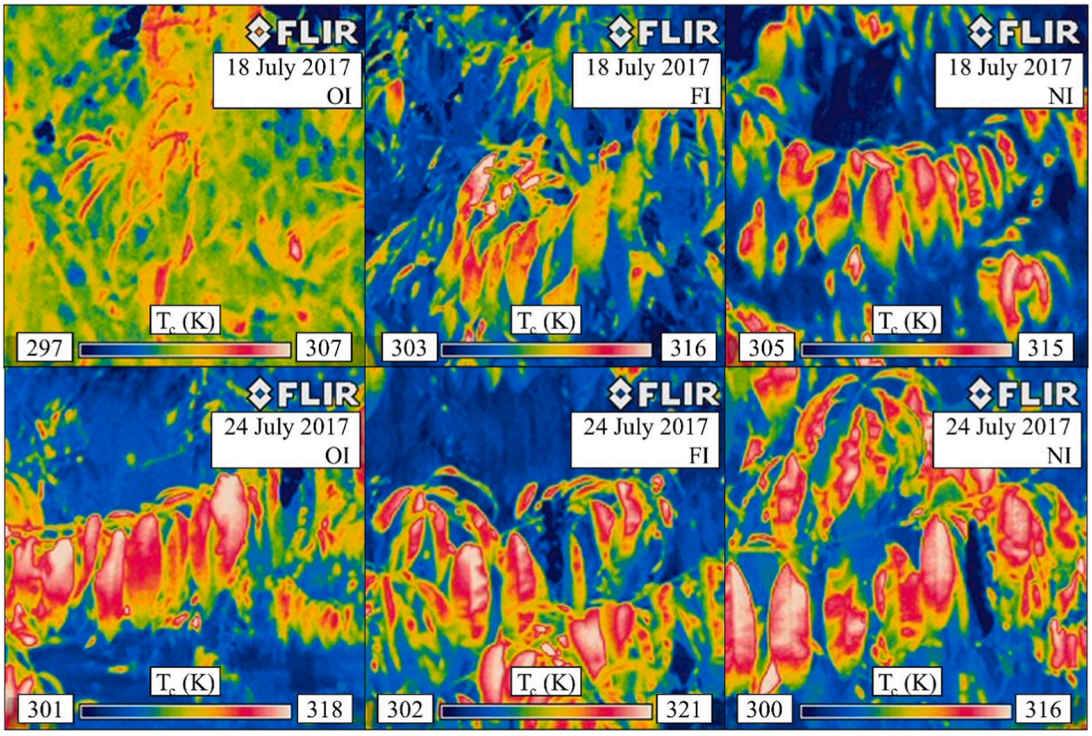

Fig. 2. Thermal imagery (K) acquired from the on-ground hand-held camera for each irrigation treatment and water status condition in 2017 (i.e. well watered: 18 July 2017; mild water stress: 24 July 2017). OI, FI and NI refer to over irrigation, farmer irrigation and non-irrigation treatments, respectively.

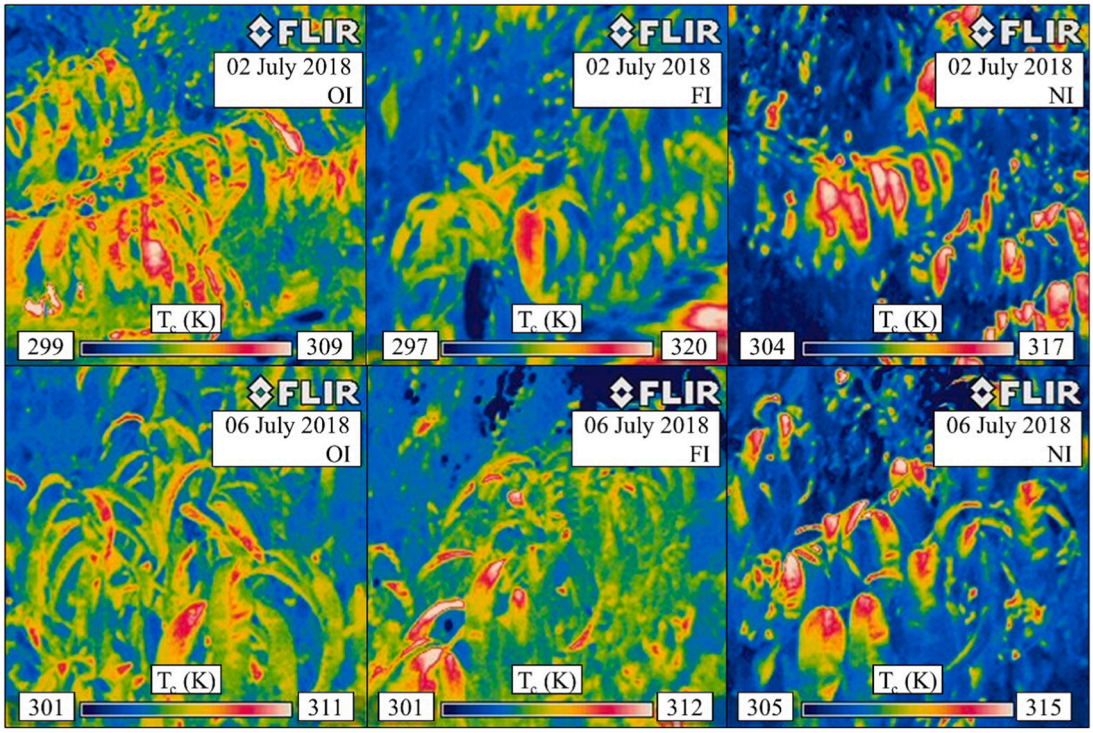

Fig. 3. Thermal imagery (K) acquired from the on-ground hand-held camera for each irrigation treatment and water status condition in 2018 (i.e. well watered: 02 July 2018; mild water stress: 06 July 2018). OI, FI and NI refer to over irrigation, farmer irrigation and non-irrigation treatments, respectively.

Additionally, $T_{c,g}$ was used in conjunction with the temperature of dry (T_d) and wet (T_w) reference leaves in order to compute CWSI ($CWSI_g$), according to Jones et al. (2002):

$$CWSI_g = \frac{T_{c,\ g} - T_w}{T_d - T_w} \quad (3)$$

Wet reference temperature (T_w) corresponds to a fully open stomata leaf, whereas a non-transpiring one with completely closed stomata was taken as the dry reference temperature (T_d). Such conditions were achieved in each sampled tree by spraying two leaves with soapy water on both sides (for T_w) and covering another two leaves in petroleum jelly (vaseline) on both sides (for T_d) (Jones et al., 2002). These leaves were captured in two images per tree (containing a wet and a dry reference each one), acquired at a distance of about 1 m from the plant canopy and an height of 1.6 m. Thus, a general T_w and T_d for each irrigation treatment was calculated as the average of the 6 individual reference T_w and T_d values.

Additionally, a hybrid CWSI ($CWSI_h$) was computed using $T_{c,g}$ and T_a, in order to consider an upper baseline higher than the maximum values of T_c actually measured. Thus, the lower baseline was the same one used for $CWSI_a$ computation (Berni et al., 2012). However, the upper baseline was re-calculated by using the relationship between the $T_{c,a}$ from each sampled tree and date (n = 36) and its corresponding $T_{c,g}$ measured on the sunlit part, resulting in a $(T_c - T_a)_u$ value of 8.71 K.

$$CWSI_h = \frac{(T_{c,g} - T_a) - (T_c - T_a)_l}{(T_c - T_a)_u - (T_c - T_a)_l} \quad (4)$$

2.3.2. Physiological determinations

Net photosynthesis (P_n), stomatal conductance (g_s) and midday stem water potential (Ψ_s) were monitored at the time of the image acquisition. Leaf gas exchange was measured on four mature sunlit leaves per sampled tree using a portable gas exchange system (LI-COR, LI-6400, Lincoln, NE, USA) with mean values of ambient photosynthetic photon flux density (PPFD) around 1800 μmol m^{-2} s^{-1}, the air flow was set to 300 mL min^{-1} and a near constant ambient CO_2 concentration of 400 μmol mol^{-1}. Regarding Ψ_s, it was monitored on one leaf per sampled tree using a pressure chamber (Soil Moisture Equipment Corp. model3000, Santa Barbara, CA, USA). The selected leaves were placed in plastic bags covered with aluminium foil for at least 1 h prior to the measurements, thus leaf water potential equalled Ψ_s (Begg and Turner, 1976).

3. Results

3.1. Canopy temperature comparison

Fig. 5 shows the comparison for all dates and trees between the T_c obtained from the hand-held thermal camera at the sunlit and shaded sides of the trees ($T_{c,g}$), and the near-nadir temperature determined from the aircraft ($T_{c,a}$). When comparing $T_{c,a}$ and $T_{c,g}$ in the sunlit and shaded sides, PBIAS values of + 0.91% and − 1.61% were obtained, respectively (Fig. 5). However, when canopy temperature measured on the ground was calculated as the average of the sunlit and shaded sides, a regression closer to the 1:1 in comparison with that derived from the aircraft was obtained, with PBIAS equals to − 0.34% (Fig. 5). Still, these comparisons showed intercept terms far from zero (53–194 K), as well as presenting some scatter in the data with RMSE values ranging from 1.67 to 5.01 K.

3.2. Assessment of the airborne- versus handheld-based CWSI as an indicator of tree water status

Fig. 6 shows the airborne CWSI ($CWSI_a$) and Ψ_s for both non-water stress (day 1) and water stress conditions (day 2) in 2017 and 2018. In day 1, OI plants had higher Ψ_s values than FI (−0.98 vs −1.27 MPa in 2017; and −1.02 vs −1.40 MPa in 2018), with NI being the treatment with the lowest Ψ_s values (−2.33 and −1.95 MPa for 2017 and 2018, respectively). However, after imposing the mild water stress (day 2), no significant differences were observed in Ψ_s between the irrigation treatments, with all of them obtaining average Ψ_s values lower than − 1.60 MPa, and reaching a minimum under these conditions of

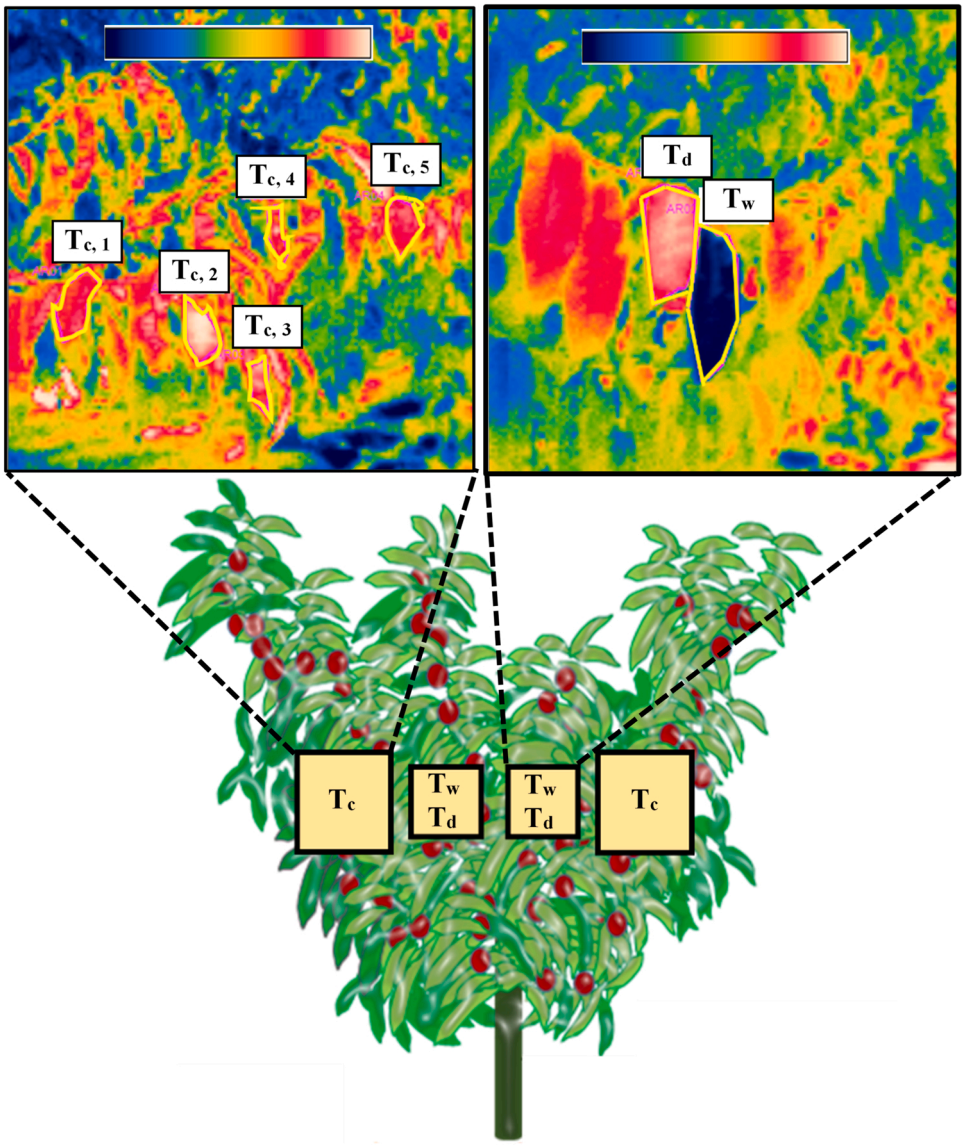

Fig. 4. Set-up of the thermal imagery acquisition with the hand-held camera. T_c refers to canopy temperature and T_w and T_d to wet and dry reference temperatures, respectively. Numerical sub-index indicates the number of leaf sample.

– 2.20 MPa for the NI treatment in 2017.

For both years, the OI treatment showed very low $CWSI_a$ values (< 0.09) on day 1, indicating non-stressed water status conditions of the plants under this irrigation strategy. A higher $CWSI_a$ value was obtained for the FI treatment on day 1, with values ranging from 0.17 to 0.24, in 2018 and 2017, respectively (Fig. 6). On the contrary, $CWSI_a$ values obtained for the NI treatment on day 1 ($CWSI_a$ from 0.39 to 0.46 in 2017 and 2018, respectively) were significatively higher than the $CWSI_a$ from OI and FI, indicating that NI trees suffered from water stress conditions from the beginning, as expected. However, when analysing $CWSI_a$ values on day 2, after withholding irrigation for 3 or 4 days, the average $CWSI_a$ for all treatments was higher than those obtained on day 1, which indicates higher water stress levels (Fig. 6). When comparing the different irrigation strategies on day 2, all the treatments reached similar values in 2017 ($CWSI_a$ varying from 0.49 to 0.54); whereas in 2018, the OI treatment still showed lower $CWSI_a$ values than FI and NI, with values of 0.23 and 0.46–0.50, respectively (Fig. 6).

When analysing the ground-based CWSI ($CWSI_g$) and the hybrid CWSI ($CWSI_h$) patterns (Figs. 7 and 8), a similar pattern to that observed from the airborne measurements was obtained on day 1, with the OI treatment yielding lower values than FI or NI, respectively; nevertheless, no significant differences were found in $CWSI_g$ on day 1 from 2017. In addition, after applying the mild water stress (day 2; Figs. 7 and 8), non-significant differences between the FI and NI treatments were obtained in terms of $CWSI_g$ (0.72–0.84; Day 2 in Fig. 7), and $CWSI_h$ (0.66–0.87; Day 2 in Fig. 8) values, whereas $CWSI_g$ and $CWSI_h$ values from the OI treatment ($CWSI_g$ of 0.52–0.57 and $CWSI_h$ of 0.34) were maintained below FI and NI, which is in accordance to the pattern observed in the $CWSI_a$ values from 2018 (Fig. 6). On the other hand, contrary to what was observed in the $CWSI_a$, the $CWSI_g$ and $CWSI_h$ had greater values for all the treatments and water stress conditions assessed (Figs. 7 and 8).

When analysing the T_c – T_a versus Vapour Pressure Deficit (VPD) data plot (Fig. 9) it can be observed that for each date, the OI treatment was the closest to the lower baseline from both the airborne and the hand-held camera results. The OI trees farthest from the lower baseline corresponded with OI trees under mild water stress conditions (day 2 of 2017 and 2018). The FI and NI treatments presented higher T_c –T_a values, but their behaviour depended on the approach used for deriving T_c. When T_c was obtained from the aircraft ($T_{c,a}$), all the FI and NI trees showed $T_{c,a} - T_a$ values always lower than the upper baseline used in this approach (5° C). Contrarily, when the hand-held camera was used for deriving T_c ($T_{c,g}$), most of the $T_{c,g}$ –T_a values of the FI and NI treatments

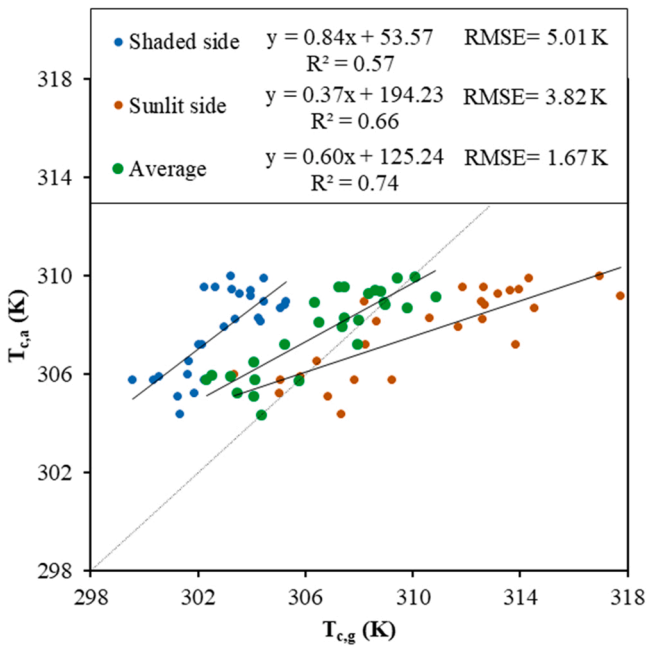

Fig. 5. Comparison of canopy temperature (T_c) of each tree (n = 27 *) for all dates obtained on the ground from the thermal hand-held camera ($T_{c,g}$) (of the sunlit and shaded sides of the tree and the average) and from the thermal sensor on board the aircraft ($T_{c,a}$). * *T_c measurements corresponding to mild water stress conditions in 2018 (n = 9) were not considered due to sensor malfunctioning when measuring the shaded sides of the trees.*

were greater than the upper baseline proposed by Irmak et al. (2000) ($T_{c,g}$ –T_a = 5.00 °C or K), but lower than the upper baseline derived for the hybrid approach ($T_{c,g}$ –T_a = 8.71 K).

When comparing the $CWSI_a$ with $CWSI_g$ and $CWSI_h$ values (Fig. 10), it was observed that the relationship obtained for both indices had an R^2 of 0.37 and 0.36 for $CWSI_g$ and $CWSI_h$, respectively. In addition, the CWSI computed from airborne data ($CWSI_a$) was always lower than the CWSI computed from ground T_c measurements ($CWSI_g$ and $CWSI_h$).

3.3. Relationships between physiological and thermal parameters

3.3.1. Stem water potential

Fig. 11 shows the relationship between Ψ_s and T_c or CWSI ($CWSI_a$, $CWSI_g$ and $CWSI_h$), with an inversely proportional pattern found for both of them. However, when analysing which variable (T_c or CWSI) and source (ground or airborne) was more appropriate for deriving Ψ_s (Fig. 11) it was observed that the most accurate Ψ_s estimates were obtained using $CWSI_a$ (R^2 of 0.72). T_c measured on the ground and $CWSI_h$ provided Ψ_s estimates with R^2 values of 0.51 and 0.58, respectively; whereas the use of T_c from the airborne measurements and $CWSI_g$ resulted in poorer accuracies (R^2 of 0.27 and 0.31, respectively).

3.3.2. Stomatal conductance

Fig. 12 shows g_s values obtained for the different irrigation strategies for both non-water stress (day 1) and water stress conditions (day 2) in 2017 and 2018. For day 1 in both years, the OI treatment obtained the highest g_s values (229–244 mmol m^{-2} s^{-1}), followed by FI (95–158 mmol m^{-2} s^{-1}) and NI (35–52 mmol m^{-2} s^{-1}), respectively. After the imposition of a mild water stress in 2017 and 2018 (day 2), it was observed that g_s decreased from day 1 to day 2 in the OI (from 244 to 168 mmol m^{-2} s^{-1} in 2017, and from 229 to 199 mmol m^{-2} s^{-1} in 2018) and FI treatments (from 95 to 58 mmol m^{-2} s^{-1} in 2017 and from 158 to 98 mmol m^{-2} s^{-1} in 2018); whereas NI remained the same or even increased. Specifically, the FI treatment reached similar values to those of the NI treatment (23–58 mmol m^{-2} s^{-1} for 2017 and 83–98 mmol m^{-2} s^{-1} for 2018); whereas OI still had significantly higher values than the other treatments (168 mmol m^{-2} s^{-1} for 2017 and 199 mmol m^{-2} s^{-1} for 2018).

Fig. 13 shows the relationship of g_s with T_c and CWSI. Stomatal conductance correlates negatively with T_c and CWSI, as expected. However, in this case, both for T_c and CWSI, the use of ground measurements provided more accurate results than using data from airborne imagery, especially in the case of $T_{c,g}$ and $CWSI_h$, with R^2 of 0.74 and 0.79, respectively. However, when data acquired from the airborne measurements was used, $CWSI_a$ (R^2 of 0.56) was preferred over the use of T_c (R^2 of 0.41) for estimating g_s.

3.3.3. Net photosynthesis

The pattern observed in P_n (Fig. 14) was the same as that for Ψ_s and g_s. In both years, for non-water stress conditions (day 1), P_n was greater

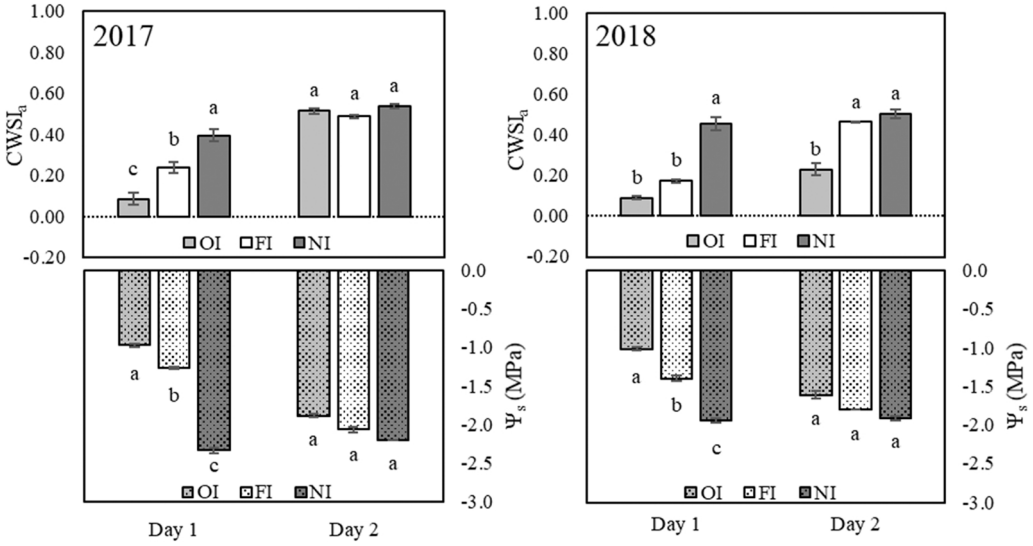

Fig. 6. Mean airborne CWSI ($CWSI_a$) and average midday stem water potential (Ψ_s, MPa) for the over-irrigation (OI; n = 3), farmer irrigation (FI; n = 3) and non-irrigation (NI; n = 3) treatments under different water stress conditions in 2017 and 2018. The error bars indicate the standard error (SE) of the average. For each year and day, different letters indicate significant differences between treatments at $p \leq 0.05$ level.

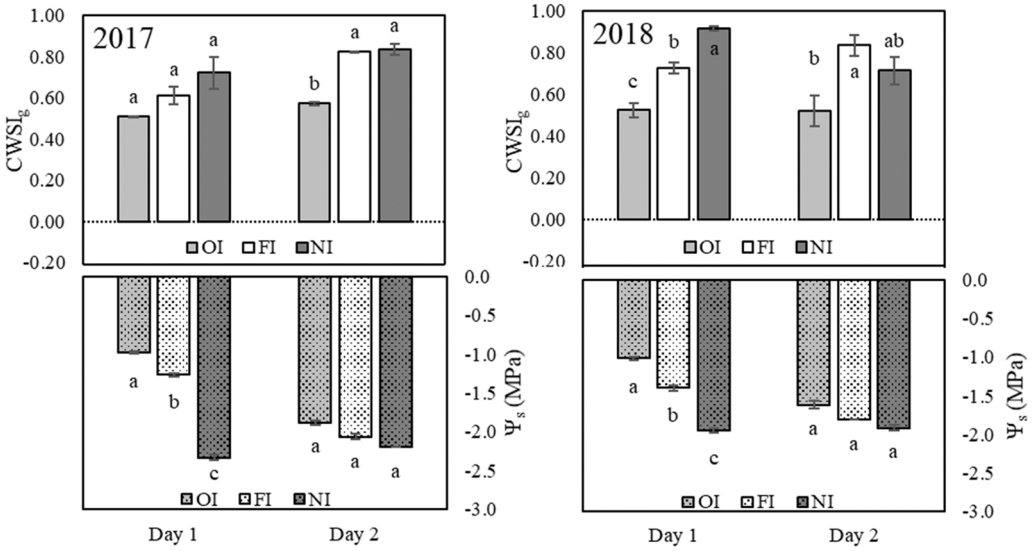

Fig. 7. Mean ground-based CWSI ($CWSI_g$) and average midday stem water potential (Ψ_s, MPa) for the over-irrigation (OI; n = 3), farmer irrigation (FI; n = 3) and non-irrigation (NI; n = 3) treatments under different water stress conditions in 2017 and 2018. The error bars indicate the standard error (SE) of the average. For each year and day, different letters indicate significant differences between treatments at $p \leq 0.05$ level.

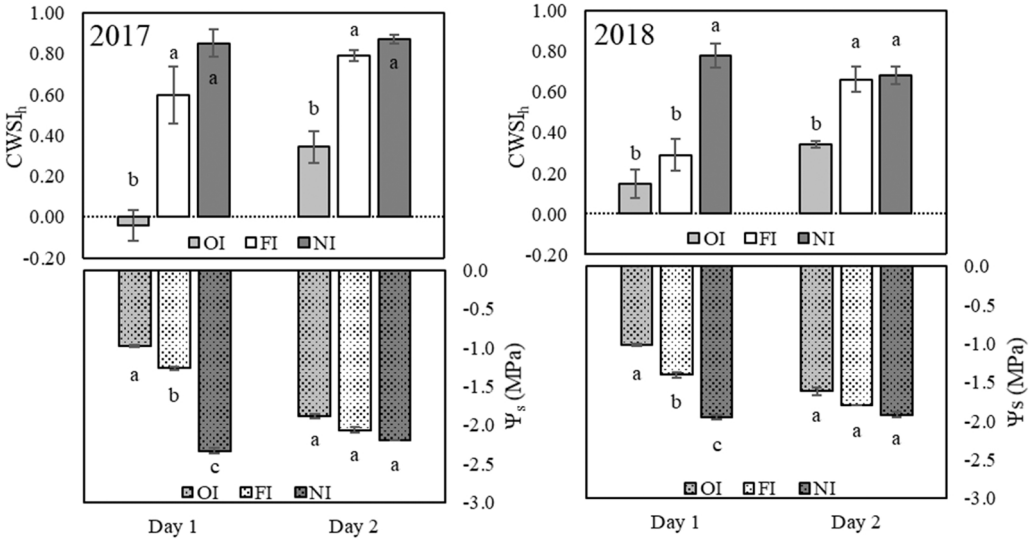

Fig. 8. Mean hybrid CWSI ($CWSI_h$) and average midday stem water potential (Ψ_s, MPa) for the over-irrigation (OI; n = 3), farmer irrigation (FI; n = 3) and non-irrigation (NI; n = 3) treatments under different water stress conditions in 2017 and 2018. The error bars indicate the standard error (SE) of the average. For each year and day, different letters indicate significant differences between treatments at $p \leq 0.05$ level.

for the OI and FI than for NI treatment, with average values ranging from 16.2 to 16.7 μmol m^{-2} s^{-1} for OI, from 8.9 to 12.5 μmol m^{-2} s^{-1} for FI, and from 3.2 to 3.3 μmol m^{-2} s^{-1} for NI. When comparing the different irrigation strategies in water stress conditions (day 2), no significant differences were observed between the FI and NI treatments, with values ranging from 2.4 to 5.4 μmol m^{-2} s^{-1} for 2017 and from 8.7 to 9.7 μmol m^{-2} s^{-1} for 2018. However, P_n values obtained for the OI treatment were significantly greater than those of FI and NI, with values close to 14.5 μmol m^{-2} s^{-1} for both years.

The relationship of P_n with T_c and CWSI followed a similar pattern than those obtained for g_s, with P_n being higher as T_c or CWSI were lower (Fig. 15). In general, T_c provided better results than using $CWSI_a$ and $CWSI_g$ for P_n estimation (R^2 of 0.73 vs 0.58 when using ground measurements; and R^2 of 0.45 vs 0.44 when using data derived from airborne measurements). Nevertheless, the use of $CWSI_h$ for P_n estimation provided similar accuracies than using ground T_c (R^2 of 0.73). In addition, the use of ground measurements (both T_c and CWSI) resulted in more accurate P_n estimates than using T_c and CWSI values obtained from the airborne ones (R^2 of 0.73 vs 0.45 for T_c and R^2 of 0.58–0.73 vs 0.44 for CWSI). Therefore, the use of ground T_c measurements and $CWSI_h$ for estimating P_n provided the most accurate estimates (R^2 of 0.73).

4. Discussion

The complexity and heterogeneity of canopy architecture, including leaf angle distribution and leaf area density, create a spatial and temporal T_c heterogeneity within plant canopies (Leinonen and Jones, 2004). Such canopy heterogeneity induces certain degree of variability in crop water status determination, depending on the canopy region considered for extracting T_c. In this sense, Ngao et al. (2017) assessed the interactions between climate, tree architecture, and plant

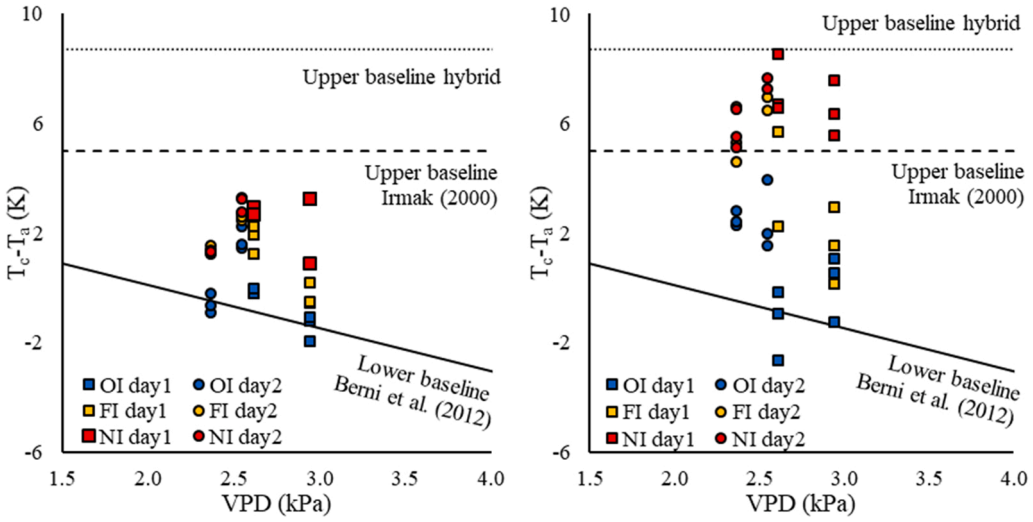

Fig. 9. Difference between canopy surface temperature (left: from the thermal sensor on board the aircraft, $T_{c,a}$; right: from the hand-held camera, $T_{c,g}$) and air temperature (T_a) as a function of observed Vapour Pressure Deficit (VPD) for days 1 and 2 in 2017 and 2018, for the over-irrigation (OI), farmer irrigation (FI) and non-irrigation (NI) treatments; and baselines used for CWSI computation.

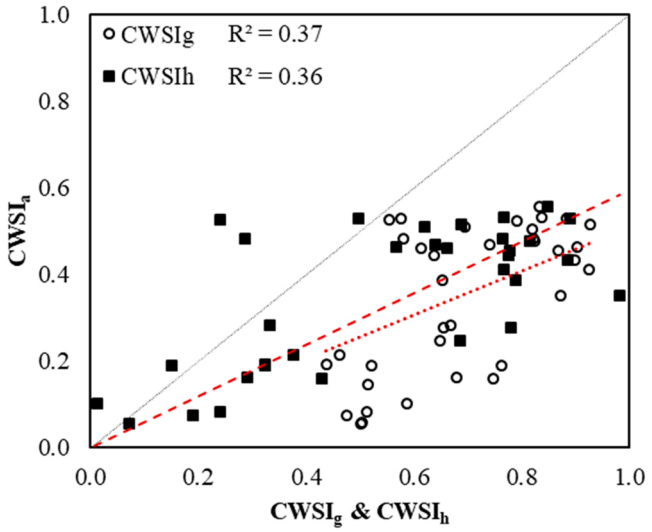

Fig. 10. Relationship between the CWSIs calculated from T_c acquired from airborne ($CWSI_a$), on the ground ($CWSI_g$) and from the hybrid approach ($CWSI_h$).

physiology in young apple trees. Specifically, these authors evidenced that in the absence of drought, the leaf temperature gradient was smaller in the upper part of the tree than for the whole crown, with the upper portion of the canopies having warmer leaves temperatures and a more random distribution. In addition, Ngao et al. (2017) observed that drought influenced the within-crown microclimate, increasing leaf spatial variability regardless of the tree position considered. Moreover, Camino et al. (2018) observed that when using the T_c from the top of the tree, derived from an UAV, out-of-range CWSI values were obtained as a consequence of the within-crown shadows and the soil background effects. For overcoming the influence of soil background, Camino et al. (2018) proposed considering uniquely thermal pixels contained in crown areas below the 50th percentile. In addition, there might be large variations in canopy temperature within a tree crown, possibly influencing the ability to detect plant water status using thermography (González-Dugo et al., 2012). This is an important issue when determining the portions of the tree crowns that should be preferentially measured and the type of instruments to be used for determining T_c.

In this study, the T_c derived from the airborne platform allowed the measurement of a high number of trees integrating the entire tree crown, including both sun-exposed and shaded areas within the canopy (Ballester et al., 2013a; b). Such T_c airborne measurements collect a more representative tree thermal status than the on-ground thermal measurements taken in specific portions of a tree crown. In fact, airborne T_c was higher than the T_c obtained from the ground data in the shaded parts of the tree (Fig. 5), and lower than that measured in the sunlit part (most exposed to the solar radiation). When averaging the ground measurements of T_c in both the sunlit and shaded parts of the tree, a relationship close to 1:1 between the two approaches was obtained. Therefore, due to the nadir view zenith angle of the sensor on board the airborne platform, a remote sensing-based approach is able to reveal the spatial within-crown T_c heterogeneity (González-Dugo et al., 2012). Such intra-crown heterogeneity is also partially feasible using handheld thermal cameras, with the inconvenience that these sensors are not able to capture both the shaded and sun-exposed parts of the crown in a single image due to its lateral view. Another disadvantage of using handheld thermal cameras is that they usually capture a single tree per image which, coupled with the variability of T_c due to external factors such as instantaneous wind or radiation variability (Ramírez-Cuesta et al., 2022), hinder the inter-tree T_c comparison. On the contrary, the use of handheld thermal cameras allows an easy T_c image acquisition without requiring much prior logistics.

When the CWSI values obtained from the different proposed approaches were compared, it was observed that they followed the same relative behaviour. Nevertheless, large differences were found when the absolute values were considered. More specifically, at initial conditions, the OI treatment was less stressed than FI and NI, respectively; and these differences were minimized after the mild water stress was imposed. This resulted in FI reaching similar CWSI values to the NI treatment, but the OI trees still showed less water stress than the other two treatments, probably due to the high soil moisture during the days previous to the stress. One exception was observed in 2017, where CWSI from OI in day 2 reached similar values than NI and FI. This was probably because in that year, there was one more day for developing the mild water stress than in 2018 (4 days in 2017 versus 3 days in 2018; Table 1). Additionally, 2017 was drier than 2018 (mean daily ET_o and cumulative P of 5.2 and 88 mm for 2017, respectively; and 5.1 and 145 mm for 2018, respectively; for the period March-August), so a lower soil water availability could be expected, which could help explaining these similar CWSI values in day 2 from 2017. However, higher CWSI values were

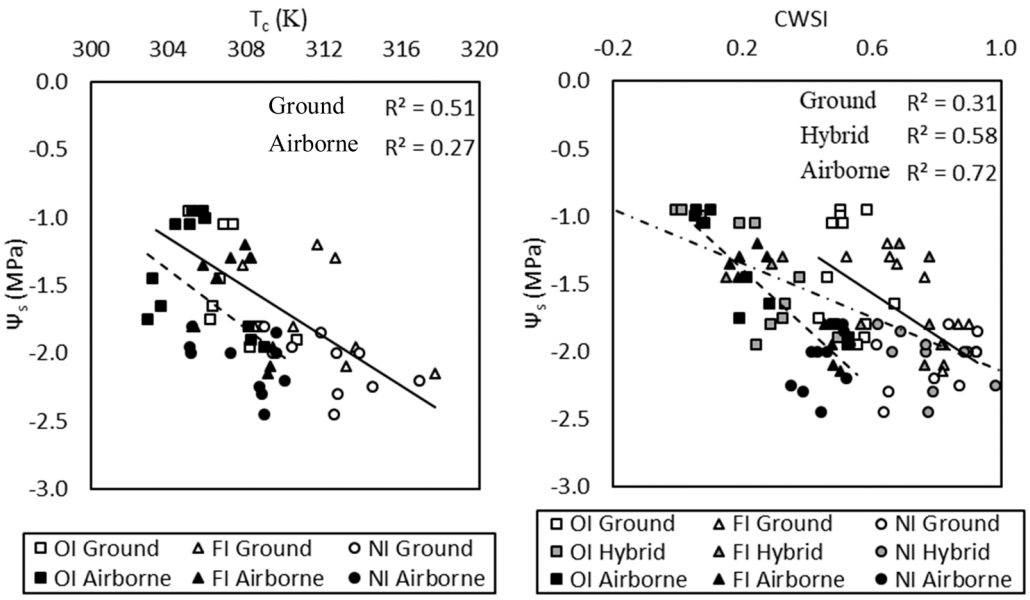

Fig. 11. Relationship between midday stem water potential (Ψ_s) and canopy temperature, T_c (left) and CWSI (right) determined from ground, hybrid and airborne approaches.

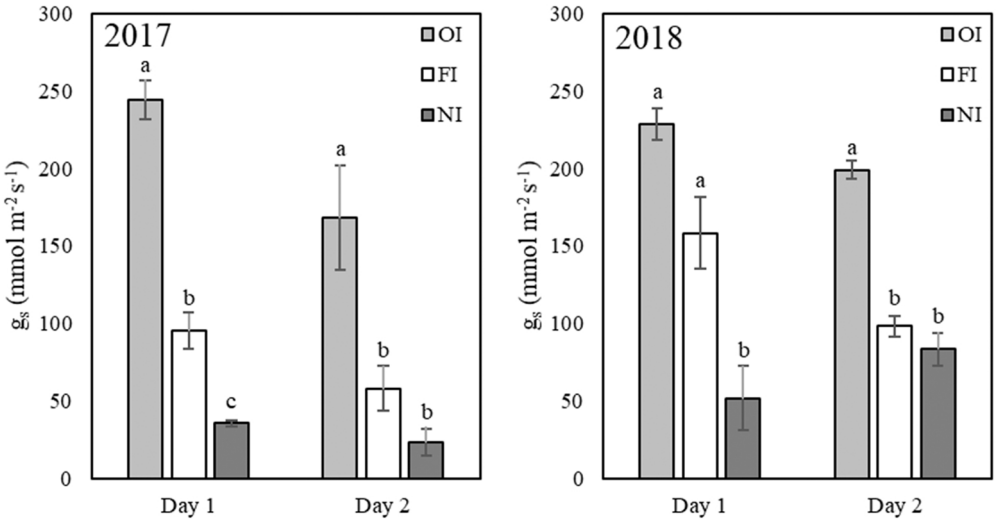

Fig. 12. Mean values of stomatal conductance (g_s) for the over-irrigation (OI; n = 3), farmer irrigation (FI; n = 3) and non-irrigation (NI; n = 3) treatments under different water stress conditions in 2017 and 2018. The error bars indicate the standard error (SE) of the average. For each year and day, different letters indicate significant differences between treatments at $p \leq 0.05$ level.

obtained from on-ground T_c measurements, even under well-watered conditions, suggesting that this approach might overestimate the crop water stress. Using on-site references particularly for obtaining T_w is a procedure influenced by experimental errors because there might be large variations in T_w within a tree canopy, and the leaf wetness level is very dynamic, particularly under warm and dry conditions (Aparecido et al., 2017). In addition, the CWSI estimation procedure using on-site wet and dry reference leaves was obtained considering the sun exposed side of the tree crown which is the portion of tree canopy with higher absolute T_c levels.

Similar responses to the water stress development than those obtained for CWSI were observed when analysing P_n, g_s and Ψ_s parameters, indicating that at initial conditions, the OI treatment was less stressed than FI and NI, respectively; whereas the differences between treatments were minimized when a short water restriction was applied. In this sense, it is important to note that, even for the FI treatment, a pre-existing stress was observed at the initial conditions as reflected by the relatively high CWSI values and the low P_n, g_s and Ψ_s values obtained at day 1 (t_0) from both years. This was probably due to the high evaporative demand at the time of image acquisition, being more evident in 2018 when daily ET_0 was greater (8.6 mm d^{-1};Table 1), and also to the adoption of mild deficit irrigation after harvest in FI, as a standard practice for early maturing stone fruit trees cultivated in the area. This fact highlights that CWSI is closely related with P_n, g_s and Ψ_s, in a manner that high T_c and CWSI values reflect the stomatal closure induced by the water stress values, which reduces P_n, g_s and Ψ_s values (Jackson et al., 1981; Jones, 1999a; b; Gonzalez-Dugo et al., 2014; Egea et al., 2017). The relationships reported here between P_n and CWSI are, however, empirical and associated to the fact that both CWSI and P_n are affected by stomatal closure. More direct estimates of canopy photosynthesis could be made from remote sensing data, using vegetation indices calculated from narrowband reflectance measurements, such as

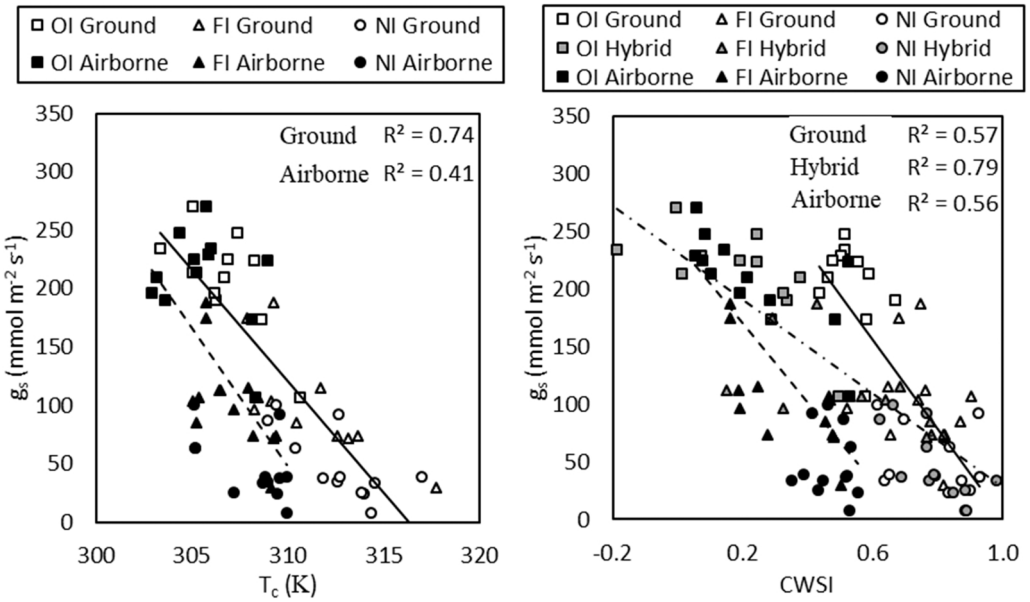

Fig. 13. Relationship between stomatal conductance (g_s) and canopy temperature, T_c (left) and CWSI (right) determined from ground, hybrid and airborne approaches.

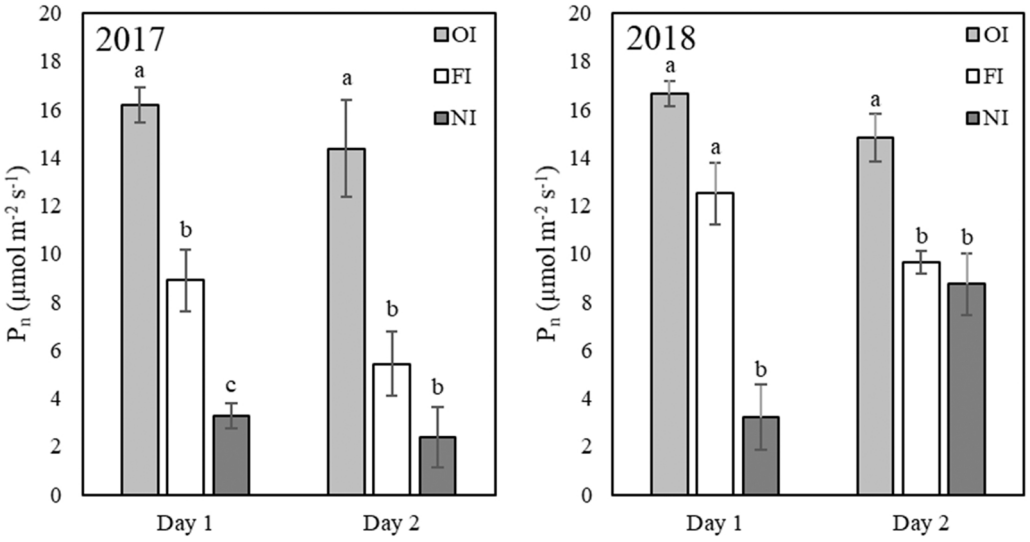

Fig. 14. Mean values of net photosynthesis (P_n) for the over-irrigation (OI; n = 3), farmer irrigation (FI; n = 3) and non-irrigation (NI; n = 3) treatments under different water stress conditions in 2017 and 2018. The error bars indicate the standard error (SE) of the average. For each year and day, different letters indicate significant differences between treatments at $p \leq 0.05$ level.

those derived from hyperspectral sensors (Stagakis et al., 2012), including fluorescence quantification (Zarco-Tejada et al., 2013a, 2013b, 2016).

However, the results derived from our study suggest that the strength of these relationships was dependent on the approach used to determine T_c and CWSI (i.e. ground vs. airborne). In general, more accurate relationships between T_c and CWSI with P_n and g_s were obtained when using data measured on-ground, which could be explained because these physiological parameters were measured on the same side of the tree (sunlit side) than T_c and CWSI from the ground. Additionally, the leaf age seems to have an influence on the results obtained, as the zenithal field of view of the thermal sensor on board the airborne mainly collects the new shoots located on the upper part of the tree crowns, whereas the ground measurements where performed on the older leaves located on the lower parts of the tree (Syvertsen, 1982; Gonzalez-Dugo et al., 2014). Other authors have also pointed out the importance of shadows on thermal studies (Bellvert et al., 2014; Ramírez-Cuesta et al., 2017), which can explain the differences between the relationships obtained from ground measurements and airborne ones. On the other hand, Ψ_s was better determined from airborne data, since this physiological parameter was less sensitive to the location of the measurement within the tree than P_n and g_s due to the "homogenization" performed when placing the sampled leaves in plastic bags covered with aluminium foil for at least 1 h prior to the measurements.

The relatively accurate relationship found between T_c with P_n, g_s and Ψ_s when ground measurements were used, confirms the use of canopy temperature as a good indicator of crop water status. Similar findings have been obtained in the literature (García-Tejero et al., 2018; Romero-Trigueros et al., 2019; Conesa et al., 2019) under similar environmental conditions than in the present study. When the climatic conditions do not differ much among the days of T_c measurement, it is possible to find good agreements between T_c itself and other indicators

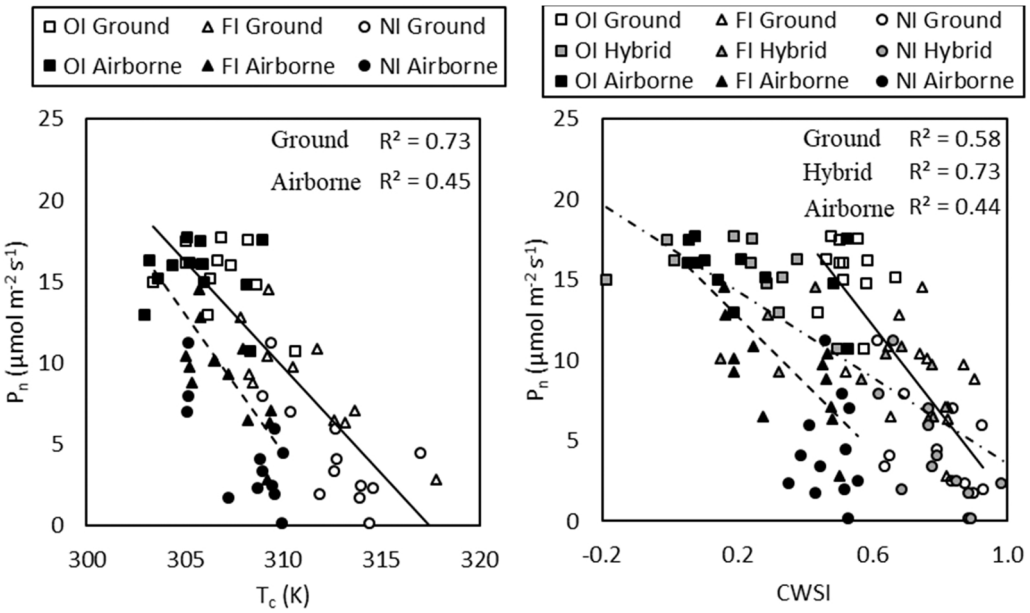

Fig. 15. Relationship between net photosynthesis (P_n) and canopy temperature, T_c (left) and CWSI (right) determined from ground, hybrid and airborne approaches.

of plant water status. However, it is still important to normalize the absolute T_c measurements by using references, to take into account the environmental conditions (Ballester et al., 2013a; b; Zarco-Tejada et al., 2012. Gonzalez-Dugo et al., 2020). The present study showed how the approach followed for normalizing T_c values was a determinant factor for a quantitative assement of crop water status over the course of given period of time.

In fact, when comparing airborne-acquired CWSI and T_c as water status indicators, it was observed that CWSI was more accurately related to the crop water status defined by Ψ_s. Similar results were reported by Gonzalez-Dugo et al. (2014) and Romero-Trigueros et al. (2019). More specifically, Gonzalez-Dugo et al. (2014) noted that the better performance of the CWSI was because it considers the evaporative demand, as well as the species-specific response of water relations to VPD. In this sense, it is remarkable that the performance of CWSI when predicting plant water status using airborne images was even better than when CWSI was obtained from on-the-ground measurements. This is despite the lower spatial resolution obtained with the airborne imagery as compared with the on-the-ground camera. To the best of our knowledge, this is the first study comparing the ability of thermal imagery to detect water stress using on-the-ground and aerial platforms. The main advantage of aerial imagery is based on its ability to measure a large surface area, which is important particularly in the case of water status assessment. Plant water status is in fact highly variable and strongly affected by environmental conditions. This implies that a few number of replicates can be measured on the ground. This is even more important when large tree-to-tree variability is observed. As in the present study, the standard error (SE) for T_c between trees from the same treatment ranged from 0.03 to 0.78 K when airborne data was used, whereas it ranged from 0.15 to 1.46 K when the on-ground approach was used. The same pattern was observed for CWSI, with SE values up to 0.03 and 0.08 for airborne and on-ground approaches, respectively. This lower variability observed between trees from the same treatment when using the aircraft imagery is due to the wider canopy proportion captured when the airborne platform was used as compared to the narrower canopy area recorded with the hand-held thermal camera. The use of a remote sensing platforms is in fact nowadays widely employed, and the present research indeed confirms its robustness when compared with simultaneous measurements on the ground.

When using only data acquired from the ground, $T_{c,g}$ provided better Ψ_s estimations than when using $CWSI_g$. This can be explained because the equation used for determining $CWSI_g$ from $T_{c,g}$ is quite dependent on the leaves used for calculating the index, especially those selected as wet and dry references and those on which the Ψ_s measurement was performed. In this sense, $CWSI_h$, with the incorporation of T_a, the lower baseline used in the airborne approach, and the re-calculation of the upper baseline, i.e. the hybrid approach, provided a closer relationship with Ψ_s than using $T_{c,g}$. Specifically, the hybrid approach uses the existing relationship between the temperature of the top and the lateral region of the trees for establishing the link between different methodologies (i.e. UAV versus handheld thermal cameras). It broadens the applicability of the thresholds used for CWSI calculation to sensors acquiring thermal images at different scales of measurement. However, special attention should be paid when directly using $T_{c,g}$ for calculating CWSI using Eq. (1), since CWSI overestimations can be obtained if the baselines, especially the upper one, are not adjusted. These overestimates are caused by higher T_c values when measured on the ground (considering only the sunny side of the tree), as opposed to those obtained from airborne-measured T_c; this suggests more stressful conditions than they actually are.

5. Conclusions

This study evaluates the feasibility of on-the-ground and airborne-based thermal indicators for identifying and quantifying the water status of a peach orchard under different irrigation regimes. CWSI values obtained from both ground and airborne platforms were able to detect peach water status under different irrigation strategies. However, whereas CWSI calculated from the aircraft integrated the entire tree crown, CWSI derived from sunlit ground T_c measurements tended to overestimate crop water stress. Special attention should be paid when combining on-the-ground and airborne-based thermal data (hybrid approach) due to the large effects caused by the baselines when computing CWSI using each method. In general, Ψ_s was better estimated from the aircraft than from ground measurement, confirming the robustness of airborne thermal imaging for large scale monitoring despite its generally lower spatial resolution. However, the use of ground measurements yielded better results than airborne thermal data when comparing against g_s and P_n, suggesting that local effects on leaf gas exchange were better captured, perhaps due to the higher spatial resolution of the proximal ground thermal sensors. Regardless the approach used for deriving T_c, CWSI provided a better relationship with

Ψ_s than using T_c, allowing for the quantitative assement of water status during the course of time-period and the integration of the effect of the climatic conditions on plant water status.

Declaration of Competing Interest

The authors declare that they have no known competing financial interests or personal relationships that could have appeared to influence the work reported in this paper.

Acknowledgments

This research was funded in the frame of the project PRECIRIEGO RTC-2017-6365-2 financed by Agencia Estatal de Investigación (AEI) with European Regional Development Fund co-funds. J.M. Ramírez-Cuesta acknowledges the postdoctoral financial support received from AEI within the Juan de la Cierva Spanish Postdoctoral Program (IJC2020-043601-I).

Appendix A. Supporting information

Supplementary data associated with this article can be found in the online version at doi:10.1016/j.agwat.2022.107628.

References

Agam, N., Cohen, Y., Berni, J.A.J., Alchanatis, V., Kool, D., Dag, A., Yermiyahu, U., Ben-Gal, A., 2013. An insight to the performance of crop water stress index for olive trees. Agric. Water Manag. 118, 79–86.
Alchanatis, V., Cohen, Y., Cohen, S., Moller, M., Sprinstin, M., Meron, M., Tsipris, J., Saranga, Y., Sela, E., 2010. Evaluation of different approaches for estimating and mapping crop water status in cotton with thermal imaging. Precis. Agric. 11 (1), 27–41.
Aparecido, L.M., Miller, G.R., Cahill, A.T., Moore, G.W., 2017. Leaf surface traits and water storage retention affect photosynthetic responses to leaf surface wetness among wet tropical forest and semiarid savanna plants. Tree Physiol. 37, 1285–1300.
Ballester, C., Castel, J., Jiménez-Bello, M.A., Castel, J.R., Intrigliolo, D.S., 2013a. Thermographic measurement of canopy temperature is a useful tool for predicting water deficit effects on fruit weight in citrus trees. Agric. Water Manag. 122, 1–6.
Ballester, C., Jiménez-Bello, M.A., Castel, J.R., Intrigliolo, D.S., 2013b. Usefulness of thermography for plant water stress detection in citrus and persimmon trees. Agric. Meteorol. 168, 120–129.
Baluja, J., Diago, M.P., Balda, P., Zorer, R., Meggio, F., Morales, F., Tardaguila, J., 2012. Assessment of vineyard water status variability by thermal and multispectral imagery using an unmanned aerial vehicle (uav). Irrig. Sci. 30, 511–522.
Begg, J.E., Turner, N.C., 1976. Crop water deficits. Adv. Agron. 28, 161–217.
Bellvert, J., Zarco-Tejada, P.J., Girona, J., Fereres, E., 2014. Mapping crop water stress index in a 'Pinot-noir'vineyard: comparing ground measurements with thermal remote sensing imagery from an unmanned aerial vehicle. Precis. Agric. 15 (4), 361–376.
Bellvert, J., Marsal, J., Girona, J., Gonzalez-Dugo, V., Fereres, E., Ustin, S.L., Zarco-Tejada, P.J., 2016. Airborne thermal imagery to detect the seasonal evolution of crop water status in peach, nectarine and Saturn peach orchards. Remote Sens. 8, 39.
Ben-Gal, A., Agam, N., Alchanatis, V., Cohen, Y., Yermiyahu, U., Zipori, I., Presnov, E., Sprintsin, M., Dag, A., 2009. Evaluating water stress in irrigated olives: correlation of soil water status, tree water status, and thermal imagery. Irrig. Sci. 27 (5), 367–376.
Berni, J.A.J., Zarco-Tejada, P.J., Sepulcre-Cantó, G., Fereres, E., Villalobos, F., 2009. Mapping canopy conductance and CWSI in olive orchards using high resolution thermal remote sensing imagery. Remote Sens. Environ. 113 (11), 2380–2388.
Berni, J.A., Zarco-Tejada, P.J., González-Dugo, V., Fereres, E., 2012. Remote sensing of thermal water stress indicators in peach. Acta Hortic. 962, 325–332.
Camino, C., Zarco-Tejada, P.J., Gonzalez-Dugo, V., 2018. Effects of heterogeneity within tree crowns on airborne-quantified SIF and the CWSI as indicators of water stress in the context of precision agriculture. Remote Sens. 10 (4), 604.
Clawson, K.L., Jackson, R.D., Pinter, P.J., 1989. Evaluating plant water stress with canopy temperature differences. Agron. J. 81, 858–863.
Cohen, Y., Alchanatis, V., Meron, M., Saranga, S., Tsipris, J., 2005. Estimation of leaf water potential by thermal imagery and spatial analysis. J. Exp. Bot. 56, 1843–1852.
Conesa, M.R., Conejero, W., Vera, J., Ramírez-Cuesta, J.M., Ruiz-Sánchez, M.C., 2019. Terrestrial and remote indexes to assess moderate deficit irrigation in early-maturing nectarine trees. Agronomy 9 (10), 630.
Costa, J.M., Grant, O.M., Chaves, M.M., 2013. Thermography to explore plant–environment interactions. J. Exp. Bot. 64 (13), 3937–3949.
Egea, G., Padilla-Díaz, C.M., Martinez-Guanter, J., Fernández, J.E., Pérez-Ruiz, M., 2017. Assessing a crop water stress index derived from aerial thermal imaging and infrared thermometry in super-high density olive orchards. Agric. Water Manag. 187, 210–221.
Fandiño, M., Olmedo, J.L., Martínez, E.M., Valladares, J., Paredes, P., Rey, B.J., Mota, M., Cancela, J.J., Pereira, L.S., 2015. Assessing and modelling water use and the partition of evapotranspiration of irrigated hop (Humulus lupulus), and relations of transpiration with hops yield and alpha-acids. Ind. Crop. Prod. 77, 204–217.
García-Tejera, O., López-Bernal, Á., Orgaz, F., Testi, L., Villalobos, F.J., 2021. The pitfalls of water potential for irrigation scheduling. Agric. Water Manag. 243, 106522.
García-Tejero, I.F., Rubio, A.E., Viñuela, I., Hernández, A., Gutiérrez-Gordillo, S., Rodríguez-Pleguezuelo, C.R., Durán-Zuazo, V.H., 2018. Thermal imaging at plant level to assess the crop-water status in almond trees (cv. Guara) under deficit irrigation strategies. Agric. Water Manag. 208, 176–186.
Gates, D.M., 1964. Leaf temperature and transpiration. Agron. J. 56, 273–277.
González-Dugo, V., Zarco-Tejada, P.J., Berni, J.A.J., Suárez, L., Goldhamer, D., Fereres, E., 2012. Almond tree canopy temperature reveals intra-crown variability that is water stress-dependent. Agric. Meteorol. 154, 156–165.
Gonzalez-Dugo, V., Zarco-Tejada, P.J., Fereres, E., 2014. Applicability and limitations of using the crop water stress index as an indicator of water deficits in citrus orchards. Agric. Meteorol. 198, 94–104.
Gonzalez-Dugo, V., Goldhamer, D., Zarco-Tejada, P.J., Fereres, E., 2015. Improving the precision of irrigation in a pistachio farm using an unmanned airborne thermal system. Irrig. Sci. 33, 43–52.
Gonzalez-Dugo, V., Zarco-Tejada, P.J., Intrigliolo, D.S., Ramírez-Cuesta, J.M., 2020. Normalization of the crop water stress index to assess the within-field spatial variability of water stress sensitivity. Precis. Agric. 1–20.
Grant, O.M., Chaves, M.M., Jones, H.G., 2006. Optimizing thermal imaging as a technique for detecting stomatal closure induced by drought stress under greenhouse conditions. Physiol. Plant 127 (3), 507–518.
Idso, S.B., Jackson, R.D., Pinter, P.J., Reginato, R.J., Hatfield, J.L., 1981. Normalizing the stress-degree day parameter for environmental variability. Agric. Meteorol. 24, 45–55.
Irmak, S., Haman, D.Z., Bastug, R., 2000. Determination of crop water stress index for irrigation timing and yield estimation of corn. Agron. J. 92 (6), 1221–1227.
Jackson, R.D., Idso, S.B., Reginato, R.J., Pinter, P.J., 1981. Canopy temperature as a crop water stress indicator. Water Resour. Res. 17, 1133–1138.
Jackson, R.D., Kustas, W.P., Choudhury, B.J., 1988. A re-examination of the crop water stress index. Irrig. Sci. 9, 309–317.
Jamshidi, S., Zand-Parsa, S., Niyogi, D., 2021. Assessing crop water stress index of citrus using in-situ measurements, Landsat, and Sentinel-2 Data. Int. J. Remote Sens. 42 (5), 1893–1916.
Jones, H.G., 1999a. Use of infrared thermometry for estimationof stomatal conductance as a possible aid to irrigationscheduling. Agric. Meteorol. 95, 139–149.
Jones, H.G., 1999b. Use of thermography for quantitative studiesof spatial and temporal variation of stomatal conductanceover leaf surfaces. Plant Cell Environ. 22, 1043–1055.
Jones, H.G., Stoll, M., Santos, T., de Sousa, C., Chaves, M.M., Grant, O.M., 2002. Use of infrared thermography for monitoring stomatal closure in the field: application to grapevine. J. Exp. Bot. 53, 2249e2260.
Jones, H.G., 2004a. Application of thermal imaging and infrared sensing in plant physiology and ecophysiology. Adv. Bot. Res. 41, 107e163.
Jones, H.G., 2004b. Irrigation scheduling: advantages and pitfalls of plant-based methods. J. Exp. Bot. 55, 2427–2436.
King, B., Shellie, K., 2016. Evaluation of neural network modeling to predict non-water-stressed leaf temperature in wine grape for calculation of crop water stress index. Agric. Water Manag. 167, 38–52.
King, B.A., Tarkalson, D.D., Sharma, V., Bjorneberg, D.L., 2021. Thermal crop water stress index base line temperatures for sugarbeet in arid western US. Agric. Water Manag. 243, 106459.
Leinonen, I., Jones, H.G., 2004. Combining thermal and visible imagery for estimating canopy temperature and identifying plant stress. J. Exp. Bot. 55 (401), 1423–1431.
Möller, M., Alchanatis, V., Cohen, Y., Meron, M., Tsipris, J., Naor, A., Ostrovsky, V., Sprintsin, M., Cohen, S., 2007. Use of thermal and visible imagery for estimating crop water status of irrigated grapevine. J. Exp. Bot. 58, 827–838.
Ngao, J., Adam, B., Saudreau, M., 2017. Intra-crown spatial variability of leaf temperature and stomatal conductance enhanced by drought in apple tree as assessed by the RATP model. Agric. . Meteorol. 237, 340–354.
Norman, J.M., Divakarla, M., Goel, N.S., 1995. Algorithms for extracting information from remote thermal-IR observations of the earth's surface. Remote Sens. Environ. 51 (1), 157–168.
Ortega-Farías, S., Ortega-Salazar, S., Poblete, T., Kilic, A., Allen, R., Poblete-Echeverría, C., Ahumada-Orellana, L., Zuñiga, M., Sepúlveda, D., 2016. Estimation of energy balance components over a drip-irrigated olive orchard using thermal and multispectral cameras placed on a helicopter-based unmanned aerial vehicle (uav). Remote Sens. 8, 638.
O'Shaughnessy, S.A., Evett, S.R., Colaizzi, P.D., Howell, T.A., 2011. Using radiation thermography and thermometry to evaluate crop water stress in soybean and cotton. Agic. Water Manag. 98, 1523–1535.
Peters, R.T., Evett, S.R., 2004. Modeling diurnal canopy temperature dynamics using one-time-of-day measurements and a reference temperature curve. Agron. J. 96, 1553–1561.
Poblete, T., Ortega-Farías, S., Ryu, D., 2018. Automatic coregistration algorithm to remove canopy shaded pixels in UAV-borne thermal images to improve the estimation of crop water stress index of a drip-irrigated Cabernet Sauvignon vineyard. Sensors 18 (2), 397.
Pou, A., Diago, M.P., Medrano, H., Baluja, J., Tardaguila, J., 2014. Validation of termal indices for water status identification in grapevine. Agric. Water Manag. 134, 60–72.
Ramírez-Cuesta, J.M., Kilic, A., Allen, R., Santos, C., Lorite, I.J., 2017. Evaluating the impact of adjusting surface temperature derived from Landsat 7 ETM+ in crop

evapotranspiration assessment using high-resolution airborne data. Int. J. Remote Sens. 38 (14), 4177–4205.
Ramírez-Cuesta, J.M., Allen, R.G., Zarco-Tejada, P.J., Kilic, A., Santos, C., Lorite, I.J., 2019. Impact of the spatial resolution on the energy balance components on an open-canopy olive orchard. Int. J. Appl. Earth Obs. Geoinf. 74, 88–102.
Ramírez-Cuesta, J.M., Consoli, S., Longo, D., Longo-Minnolo, G., Intrigliolo, D.S., Vanella, D., 2022. Influence of short-term surface temperature dynamics on tree orchards energy balance fluxes. Precis. Agric. 1–19.
Reddy, B.K., Angira, B., Blaser, B.C., Stewart, B.A., 2015. Transpiration efficiency of grain sorghum and maize under different planting geometries. J. Crop. Improv. 29, 619–635.
Romero-Trigueros, C., Bayona-Gambín, J.M., Nortes-Tortosa, P., Alarcón-Cabañero, J.J., Nicolás-Nicolás, E., 2019. Determination of crop water stress index by thermometry in grapefruit trees irrigated with saline reclaimed water combined with deficit irrigation. Remote Sens. 11 (7), 757.
Santesteban, L., Di Gennaro, S., Herrero-Langreo, A., Miranda, C., Royo, J., Matese, A., 2017. High-resolution uav-based thermal imaging to estimate the instantaneous and seasonal variability of plant water status within a vineyard. Agric. Water Manag. 183, 49–59.
Sepulcre-Cantó, G., Zarco-Tejada, P.J., Jiménez-Muñoz, J.C., Sobrino, J.A., De Miguel, E., Villalobos, F.J., 2006. Detection of water stress in an olive orchard with thermal remote sensing imagery. Agric. . Meteorol. 136 (1–2), 31–44.
Sepúlveda-Reyes, D., Ingram, B., Bardeen, M., Zúñiga, M., Ortega-Farías, S., Poblete-Echeverría, C., 2016. Selecting canopy zones and thresholding approaches to assess grapevine water status by using aerial and ground-based thermal imaging. Remote Sens 8, 822.
Shackel, K., Moriana, A., Marino, G., Corell, M., Pérez-López, D., Martin-Palomo, M.J., Caruso, T., Marra, F.P., Agüero Alcaras, L.M., Milliron, L., Rosecrance, R., Fulton, A., Searles, P., 2021. Establishing a reference baseline for midday stem water potential in olive and its use for plant-based irrigation management. Front. Plant Sci. 2715.
Sobrino, J.A., Julien, Y., García-Monteiro, S., 2020. Surface temperature of the planet earth from satellite data. Remote Sens. 12 (2), 218.
Stagakis, S., González-Dugo, V., Cid, P., Guillén-Climent, M.L., Zarco-Tejada, P.J., 2012. Monitoring water stress and fruit quality in an orange orchard under regulated deficit irrigation using narrow-band structural and physiological remote sensing indices. ISPRS J. Photogramm. Remote Sens. 71, 47–61.
Starr, G.C., 2005. Assessing temporal stability and spatial variability of soil water patterns with implications for precision water management. Agric. Water Manag. 72 (3), 223–243.
Steduto, P., Hsiao, T.C., Fereres, E., Raes, D., 2012. Crop Yield Response to Water. FAO Irrigation and Drainage Paper 66. FAO, Rome, Italy.
Syvertsen, J.P., 1982. Minimum leaf water potential and stomatal closure in citrus leaves of different ages. Ann. Bot. 49 (6), 827–834.
Tanner, C.B., 1963. Plant temperatures. Agron. J. 55, 210–211.
Wan, Z., 2014. New refinements and validation of the collection-6 MODIS land-surface temperature/emissivity product. Remote Sens. Environ. 140, 36–45.
Zarco-Tejada, P.J., González-Dugo, V., Berni, J.A., 2012. Fluorescence, temperature and narrow-band indices acquired from a UAV platform for water stress detection using a micro-hyperspectral imager and a thermal camera. Remote Sens. Environ. 117, 322–337.
Zarco-Tejada, P.J., Morales, A., Testi, L., Villalobos, F.J., 2013a. Spatio-temporal patterns of chlorophyll fluorescence and physiological and structural indices acquired from hyperspectral imagery as compared with carbon fluxes measured with eddy covariance. Remote Sens. Environ. 133, 102–115.
Zarco-Tejada, P.J., Catalina, A., González, M.R., Martín, P., 2013b. Relationships between net photosynthesis and steady-state chlorophyll fluorescence retrieved from airborne hyperspectral imagery. Remote Sens. Environ. 136, 247–258.
Zarco-Tejada, P.J., González-Dugo, M.V., Fereres, E., 2016. Seasonal stability of chlorophyll fluorescence quantified from airborne hyperspectral imagery as an indicator of net photosynthesis in the context of precision agriculture. Remote Sens. Environ. 179, 89–103.